THE ASTROPHYSICAL JOURNAL, 508:744–751, 1998 December 1

HUBBLE SPACE TELESCOPE IMAGING OF IRAS 17441−2411: A CASE STUDY OF A BIPOLAR NEBULA WITH A CIRCUMSTELLAR DISK[1]

KATE Y. L. SU, KEVIN VOLK, AND SUN KWOK[2]
Department of Physics and Astronomy, University of Calgary, Calgary, Canada T2N 1N4

AND

BRUCE J. HRIVNAK
Department of Physics and Astronomy, Valparaiso University, Valparaiso, IN 46383
Received 1998 June 22; accepted 1998 July 6

ABSTRACT

The bipolar proto–planetary nebula IRAS 17441−2411 (the "Silkworm Nebula") was observed with the *Hubble Space Telescope*. By fitting the observed spectral energy distribution and the *V*-band image by a two-dimensional radiation transfer model, we derive the properties of the circumstellar wind and a proposed circumstellar "disk." We suggest that bipolar structures are probably more common than actually observed, because objects with similar intrinsic structures may simply appear stellar because of their orientation in the sky.

Subject headings: circumstellar matter — planetary nebulae: general — stars: AGB and post-AGB

1. INTRODUCTION

Circumstellar disks are common both in young stars and evolved stars. The most widely used method of their detection is by direct imaging, mostly in the infrared but also by millimeter-wave techniques (Ohashi et al. 1991). Since the disk is often embedded in a circumstellar dust envelope, imaging in the visible is often not considered to be practical. However, the presence of a disk can be inferred and its geometry measured by the morphology of the reflection nebulae formed around the disk. If the disk is viewed edge-on, the bright central star is usually obscured by the circumstellar disk, while the visible photons that escape through the polar openings and are scattered by the circumstellar dust can form a bipolar nebula, which can be imaged. Since optical imaging is much more sensitive and has higher dynamic range than other techniques, faint reflection nebulae can be found at visible wavelengths by modern detectors. With the *Hubble Space Telescope* (*HST*), optical imaging offers higher angular resolution than the best millimeter-wave interferometry array can presently offer. In this paper, we report *HST* imaging observations of a bipolar proto–planetary nebula (PPN) and derive the properties of its circumstellar disk by comparison with a two-dimensional radiation transfer model.

2. IRAS 17441−2411 AS A PROTO–PLANETARY NEBULA

IRAS 17441-2411 (or AFGL 5385, the "Silkworm Nebula") was identified as a bipolar PPN by Kwok et al. (1996). A ground-based $V-I$ color image reveals the presence of a "disk" at the waist of the two bipolar lobes. Molecular hydrogen emission was detected by Weintraub et al. (1998), who concluded that the H_2 emission comes from the waist of the bipolar nebula. Its spectral energy distribution shows two separate peaks due to the dust and photospheric components. A *B*-band image of the object by Bobrowsky, Meixner, & Skinner (1998) suggests that the two lobes are curved and have a point-symmetric structure.

The *IRAS* LRS spectrum of IRAS 17441−2411 shows no obvious spectral features and is consistent with the dust being amorphous carbon. A circumstellar CO envelope expanding at 15 km s^{-1} was found by Hu et al. (1994). We therefore believe the circumstellar chemistry is carbon-rich, not unlike the many carbon-rich PPNs found by Kwok and Hrivnak in their program to search for PPN among cool *IRAS* sources (see Kwok 1993; Hrivnak 1997).

The observed bipolar nebulosity probably developed after the star left the asymptotic giant branch (AGB) and is the result of a fast wind opening two "holes" in the less dense parts of the asymmetric AGB envelope. Stellar visible photons escaping through these polar openings are scattered by circumstellar dust to create the bipolar morphology. The denser parts of the envelope in the equatorial directions are not visually bright because of dust absorption. The absorbed starlight is reprocessed into infrared photons by dust, giving the large infrared excess observed in this object. The nature of bipolar PPNs has been discussed in a paper on IRAS 17150−3224 (the "Cotton Candy Nebula") by Kwok, Su, & Hrivnak (1998).

3. OBSERVATIONS

Using the Wide-Field Planetary Camera 2 (WFPC2) of the *HST*, we have imaged IRAS 17441−2411 through a wide-band filter centered at 606 nm (F606W). The data were obtained in 1997 April as part of the *HST* Cycle 6 operation (program ID 6565). A total of nine exposures (4×10 s, 4×120 s, and 1×200 s) were taken. None of the pixels are saturated within the nebula even in the longest exposure frame. Standard bias subtraction, dark subtraction, and flat-fielding were performed. Since the WFPC2 undersamples the image, the technique of linear recombination of images ("drizzling;" Fruchter & Hook 1997) was used to reconstruct the point-spread function (PSF). The PSF after drizzling is found to have a FWHM of 0.″07.

To take advantage of the spatial gain available by drizzling, we took our data in a four-point dithered pattern. Each target has four similar exposures, but each is centered

[1] This work was based on observations with the NASA/ESA *Hubble Space Telescope*, obtained at the Space Telescope Science Institute, which is operated by AURA, Inc., under NASA contract NAS 5-26555.

[2] Visiting Scientist, Smithsonian Astrophysical Observatory.

at a position that differs from the others by a small, noninteger number of pixels. Cosmic rays were removed as part of the dithering processing, using the task BLOT in the Drizzle (v1.1) package.

4. RESULTS

Figure 1 shows the reduced images of IRAS 17441−2411. The image covers the central 140 × 140 pixels of the original 800 × 800 image. We can see that the lobes are resolved into several blobs of bright structure; most interestingly, the two blobs connected in the southern lobe show a footprint-like shape. In addition, a point-symmetric S-shape structure can be seen if one traces only the brighter parts of the lobes.

The sizes of the two lobes in the main nebula, as measured to ∼2% of peak flux of the north lobe, are similar, 1.″90 × 1.″64 (±0.″02). Using this size as an elliptical aperture, we obtain a total integrated flux of $m(606) = 15.75$ mag from the north lobe, and $m(606) = 16.41$ mag from the south lobe, giving a flux ratio of 1.84 between the two lobes. To obtain the total flux from the entire nebula, we used an elliptical aperture of size 6.″4 × 5.″2, which extends to the level of ∼1% of the peak flux of the north lobe. After excluding the contribution from several bright stars within the aperture, we arrive at an total integrated flux of $m(606) = 15.14$ mag. These values were not transformed to the Johnson V system because of the documented uncertainty in this procedure (Casertano 1997). The intensity ratio (north/south) of the maximum peaks of the two lobes is ∼2.03. Assuming axial symmetry in the system, the fact that the northern lobe is brighter than the southern lobe suggests that the southern lobe suffers from more dust extinction, and the northern lobe is tilted toward us.

Faint extended structure beyond the two lobes is outlined in Figure 2. The contours were created by averaging the image in 8 × 8 pixel blocks in order to reveal the faint extended emission. This "halo" can be seen covering an area of 7.″8 × 4.″1.

Also seen in Figure 1 are two circular arcs lying beyond the main lobes of the nebula and hints of two more, one within and one beyond the lobes. By assuming the two arcs represent parts of concentric circles, we can define the center of the nebula to be $\alpha_{J2000} = 17^h47^m13^s.49$, $\delta_{J2000} = -24°12'51''.0$, which presumably represents the position of the hidden central star. We calculate the radii of the two arcs to be 1.″98 and 2.″58. These arcs are similar to ones observed in the bipolar PPNs AFGL 2688 (Sahai et al. 1998) and IRAS 17150−3224 (Kwok et al. 1998) and can be interpreted as the remnants of the circumstellar envelope ejected during the AGB phase. These probably represent intervals of enhanced mass loss. While only two arcs are seen in IRAS 17441−2411, as compared with at least seven

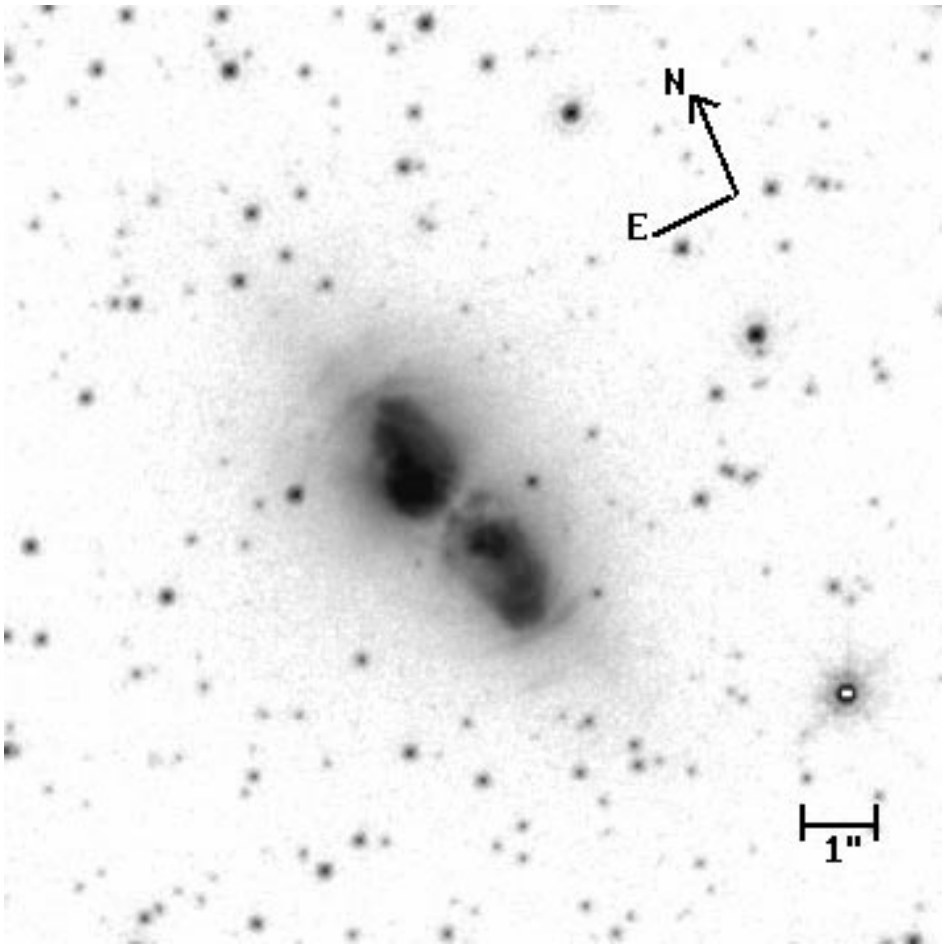

FIG. 1.—*HST*/WFPC2 F606W image of the Silkworm Nebula. Total exposure time is 480 s. The image has been deconvolved using the maximum entropy method.

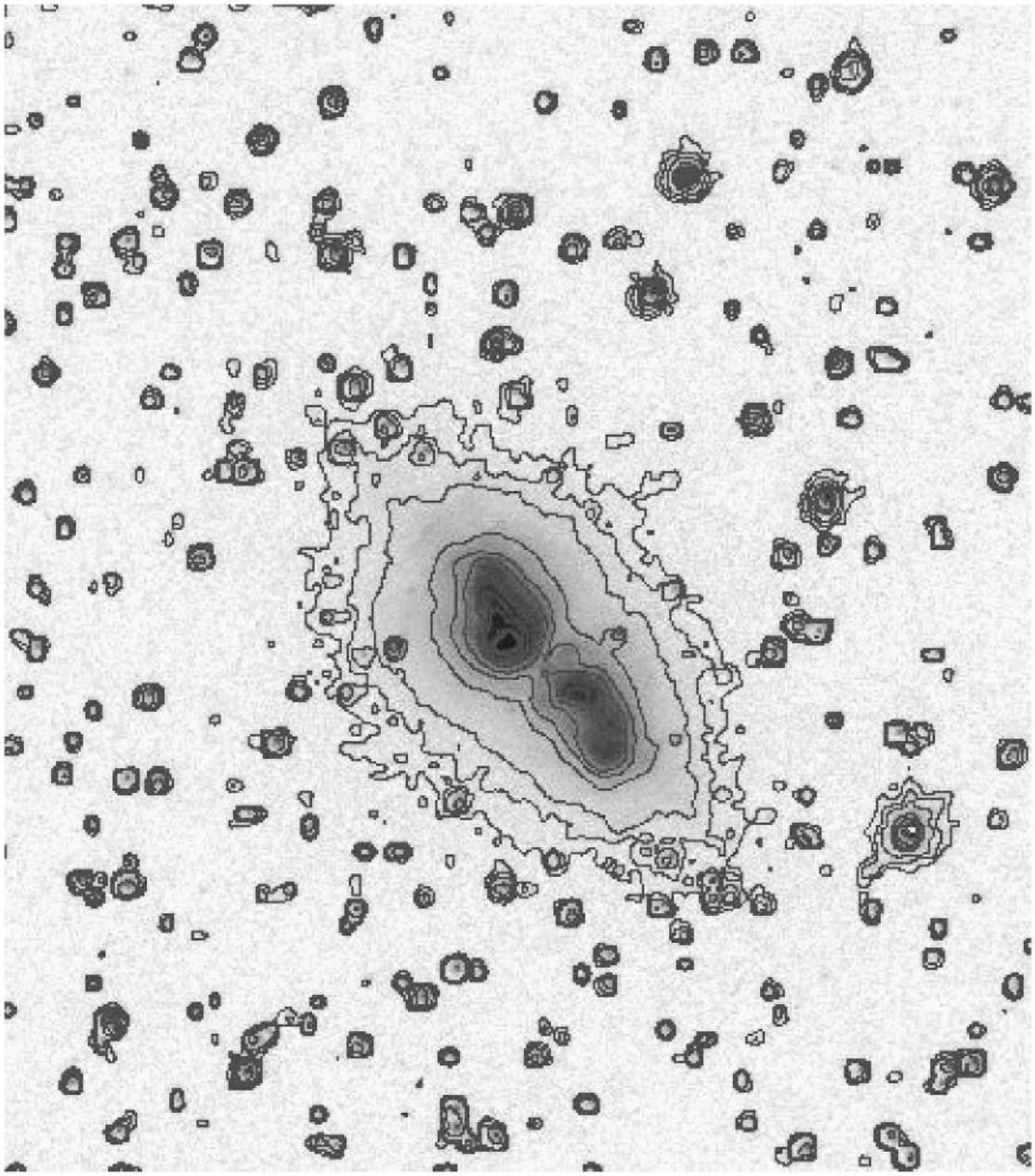

FIG. 2.—Contour plot to show the extent of the halo. The contours are created by averaging the image in 8 × 8 pixel blocks and subtracting the background. The contour levels are 21.27, 20.96, 20.52, 19.33, 18.46, 17.71, 16.71, 16.27, 15.96, 15.60, and 15.45 mag arcsec^{-2}.

in IRAS 17150−3224 and even more in AFGL 2688, we suspect that this is simply because IRAS 17441−2411 is fainter. Note that the short exposure image of IRAS 17150−3224 shows only two arcs (Kwok et al. 1998). Since our *HST* exposure times were the same for IRAS 17441−2411 and for IRAS 17150−3224, but the former is 1 mag fainter, we expect that longer exposure times would reveal more arcs. The separation of the two brighter arcs is $\sim 0\farcs6$, which corresponds to 0.003 pc (D/kpc) in physical distance or 190 yr (D/kpc) (V/15 km s^{-1})$^{-1}$ in time.

We name IRAS 17441−2411 the "Silkworm Nebula," not only for its appearance but also for the scientific connotation that the two lobes are breaking out of the AGB envelope as butterflies emerging from cocoons during their metamorphosis.

5. THE MODEL

While many PPN candidates show similar spectral shapes in the mid-IR, they have vastly different ratios of optical to mid-IR flux. This difference has been explained by Hrivnak & Kwok (1991) as the result of PPN with nonspherically symmetric envelopes being viewed from different orientations. The visually bright ones are likely to be systems viewed pole-on, while the optically faint ones are viewed edge-on. In extreme edge-on cases where the central star is totally obscured by circumstellar dust, scattered light from the circumstellar regions can be seen. In this paper, we use the observed optical morphology of IRAS 17441−2411 to infer the matter distribution in its envelope and its orientation in the sky.

While numerical solutions of the one-dimensional dust continuum radiation transfer problem has been well developed since the 1970s, a complete self-consistent solution to the two-dimensional axial-symmetric problem is much more difficult (Spagna, Leung, & Egan 1991). However, the source morphology at various wavelengths is primarily determined by geometry and density distribution and only to a lesser extent by the source function. In our current model, we obtain approximate solutions to the source function by first obtaining the dust temperature distribution from results of one-dimensional models for the "polar" and "equatorial" directions and interpolating between them. This works in both the optically thin and optically thick limits. In the former case the dust is heated only by the central star, and in the latter case local effects dominate the source function. The only assumption introduced is therefore the shape of the interpolating function. We also assume that single scattering of the starlight represents the only contribution to the scattering source function. These two approximations greatly simplify the problem and allow large numbers of models to be run within reasonable amounts of time.

For the geometry of the circumstellar envelope, we assume axial-symmetry (quantities independent of the angle ϕ) and symmetry under reflection about the equatorial plane. The density distribution in the radial direction is assumed to be r^{-2}. Input parameters are the following: the optical depths at the pole and the equator (τ_1 and τ_2, respectively), the angle of view i, the stellar temperature and flux (T_* and $L_*/4\pi D^2$, respectively), the mass-loss rate ($\dot{M}/V$), and the inner radius ($r_{\rm in}$) of the dust envelope. A total of 160 frequency grid points (ν_i), 202 radial grid points (r_i), and 18 angular grid points (θ_i) grid points are used. Interpolation in both temperature and optical depth is given by

$$T(\theta) = T_1 + (T_2 - T_1)(2\theta/\pi)^N , \quad (1)$$

$$\tau(\theta) = \tau_1 + (\tau_2 - \tau_1)(2\theta/\pi)^N , \quad (2)$$

for $0 \leq \theta \leq \pi/2$, with T_1 and τ_1 being the values of at the pole ($\theta = 0$) and T_2 and τ_2 being the values at the equator ($\theta = \pi/2$). The power index N is a free parameter. After the source function is determined at every point, the emergent intensity at various impact parameters and angles is obtained by integrating the equation of transfer along the line of sight. This produces a 1001 × 1001 image at each frequency. The flux (F_ν) is obtained by integrating over the entire image. Details of the model are discussed elsewhere (Volk et al. 1999).

5.1. *Fitting Procedure*

We apply the model to IRAS 17441−2411 by first fitting the spectral energy distribution (SED). The inner radius of the dust shell can be determined from the *IRAS* broad-band colors, since the peak of the infrared spectrum dictates the maximum dust temperature in the envelope. Once this has been determined, the τ values are varied along with the N value to fit the SED. We expect the dust component to be optically thin and its flux distribution not to be sensitive to i. When a satisfactory fit to the infrared part of the SED is obtained, these parameters are then used to calculate the intensity distribution of the envelope both in scattered and emitted light. The ratio of brightness between the two optical lobes is used to constrain our angle of view. This ratio would be unity if the system were viewed exactly edge-on ($i = 90°$), and it deviates increasingly from 1 as i decreases and one of the lobes gradually becomes more obscured by dust. As can be seen from the optical image of the Silkworm Nebula, the system is very close to being viewed edge-on.

The central star, the only energy source in the system, is assumed to be a blackbody of temperature 6000 K. The spectral type of the star has not been determined but is assumed to be of approximately G0, in common with most of the other PPNs that we have studied. The effective temperature of the star is constrained by the observed shape of the photospheric component. The fit to the dust component is not very sensitive to the stellar parameters, since the entire density distribution can be scaled to different $r_{\rm in}$ values by keeping $L_*/r_{\rm in}^2$ constant. The energy is found to be conserved to within 0.5%, thereby giving us confidence that the results are correct.

The model parameters are listed in Table 1. The conversion of the dust optical depths to mass-loss rates is done assuming a gas-to-dust mass ratio of 320 for the amorphous carbon dust. The derived mass-loss rates, given the distance uncertainties, are comparable to those observed in late-AGB stars. The observed SED of IRAS 17441−2411 and the SED produced by the model are plotted together in Figure 3. The three peaks in the model SED are, respectively, the dust component (in the mid-IR), the reddened photosphere (in the near-IR), and the scattered light from the lobes (in the visible). Note that the effect of interstellar absorption has not been included in the comparison of the observed and model curves. An approximate value of $A_V \approx 2 \pm 1$ mag is derived from the study of Neckel & Klare (1980), which, if corrected for, would raise the observed V energy near to the model curve.

5.2. *The Disk*

The two lobes of IRAS 17441−2411 are clearly separated by a central dust lane, behind which the central star is hidden. We found it difficult to reproduce such a thin dark lane between two reflection nebulae in a "pure wind" model. In order to completely hide the central star, a relatively high visual optical depth needs to be assumed, which results in a wide dark lane between the two lobes. This suggests the presence of a "disk" of high optical depth in addition to the remnant of the AGB wind. By a "disk," we mean a volume of enhanced density of limited radial extent and limited angular extent on both sides of the equator. The model parameters of the "disk" used to produce the simulated image are given in Table 1. Physically, this "disk" could be the result of a limited period of enhanced mass loss concentrated in the equatorial plane.

Figure 4 shows the model image of IRAS 17441−2411 in the V band. While the simple model does not fit the small-scale structure of the detailed *HST* image, it does give a reasonable fit to the brightness distribution in the V band, while at the same time giving an excellent fit to the SED in the mid- and far-IR.

5.3. *Derived Parameters*

Table 2 lists comparisons between the observed and model *IRAS* colors for IRAS 17441−2411. The *IRAS* colors are calculated using the formulae defined by Kwok, Volk, & Bidelman (1997). We have matched the [12]−[25] and [25]−[60] colors within their uncertainties and also

TABLE 1

MODEL PARAMETERS

Parameter	Value
Envelope Parameters[a]	
$\dot{M}_1$	5.66×10^{-6} (D/1 kpc) (V/15 km s^{-1}) $M_\odot$ yr^{-1}
$\dot{M}_2$	$10\dot{M}_1$
$\langle\dot{M}\rangle$	4.54×10^{-5} (V/15 km s^{-1})(D/1 kpc) $M_\odot$ yr^{-1}
τ_1(11.22 μm)	0.005
τ_2(11.22 μm)	0.05
r_{in}	0.00268 (D/1 kpc) pc
r_{out}	0.26 (D/1 kpc) pc
$T_{d,1}(r_{in})$	194 K
$T_{d,2}(r_{in})$	198 K
N	0.5
Disk Parameters	
ρ_{disk}/ρ_{wind}	20
Disk opening angle	$\pm 5°$ (from "equator")
Disk outer radius	0.0081 (D/1 kpc) pc ($=3 \times r_{in}$)
Enhanced mass loss rate $\langle\dot{M}\rangle$	1.38×10^{-4} (D/1 kpc) (V/15 km s^{-1}) $M_\odot$ yr^{-1}
Duration of enhanced mass loss	393 (D/1 kpc) (V/15 km s^{-1})$^{-1}$ yr
Geometry and Stellar Parameters	
i	86°
T_*	6000 K
L_*	6300 $L_\odot$(D/2.0 kpc)^2

a Note that the subscripts 1 and 2 refer to the polar ($\theta = 0°$) and equatorial ($\theta = 90°$) values, respectively.

TABLE 2

MODEL RESULTS

Quantity	Observed Value	Model Value
[12] − [25]	3.21 ± 0.10	3.13
[25] − [60]	1.31 ± 0.16	1.39
[60] − [100]	<0.29	0.32

have a [60]−[100] value that is consistent with the observed upper limit given the uncertainty in the 60 μm flux density. By fitting the observed 12 μm flux by the model, we estimate a distance of 2.0 $(L_*/6300\ L_\odot)^{1/2}$ kpc for 17441−2411. This differs somewhat ($\sim$30%) from the distance calculated in our earlier paper (Kwok et al. 1996), because a simple summing of the observed fluxes underesti-

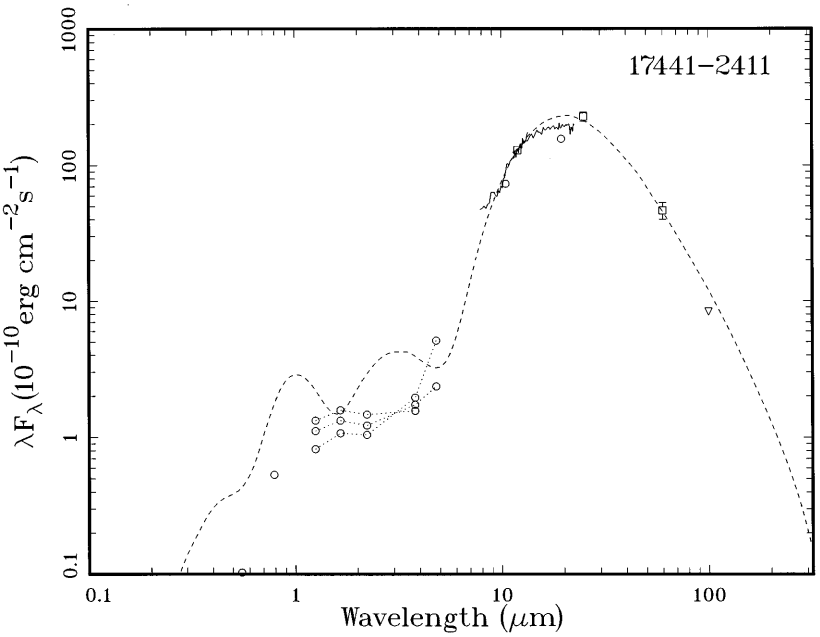

FIG. 3.— SED of 17441−2411 fitted by a two-dimensional radiation transfer model. The orientation angle is 86°. Visible and near-IR observations are from Kwok et al. (1996), with additional near-IR observations from Hu et al. (1993) and P. Whitelock (1988, private communication). Also shown at the longer wavelengths are the *IRAS* photometry and spectra.

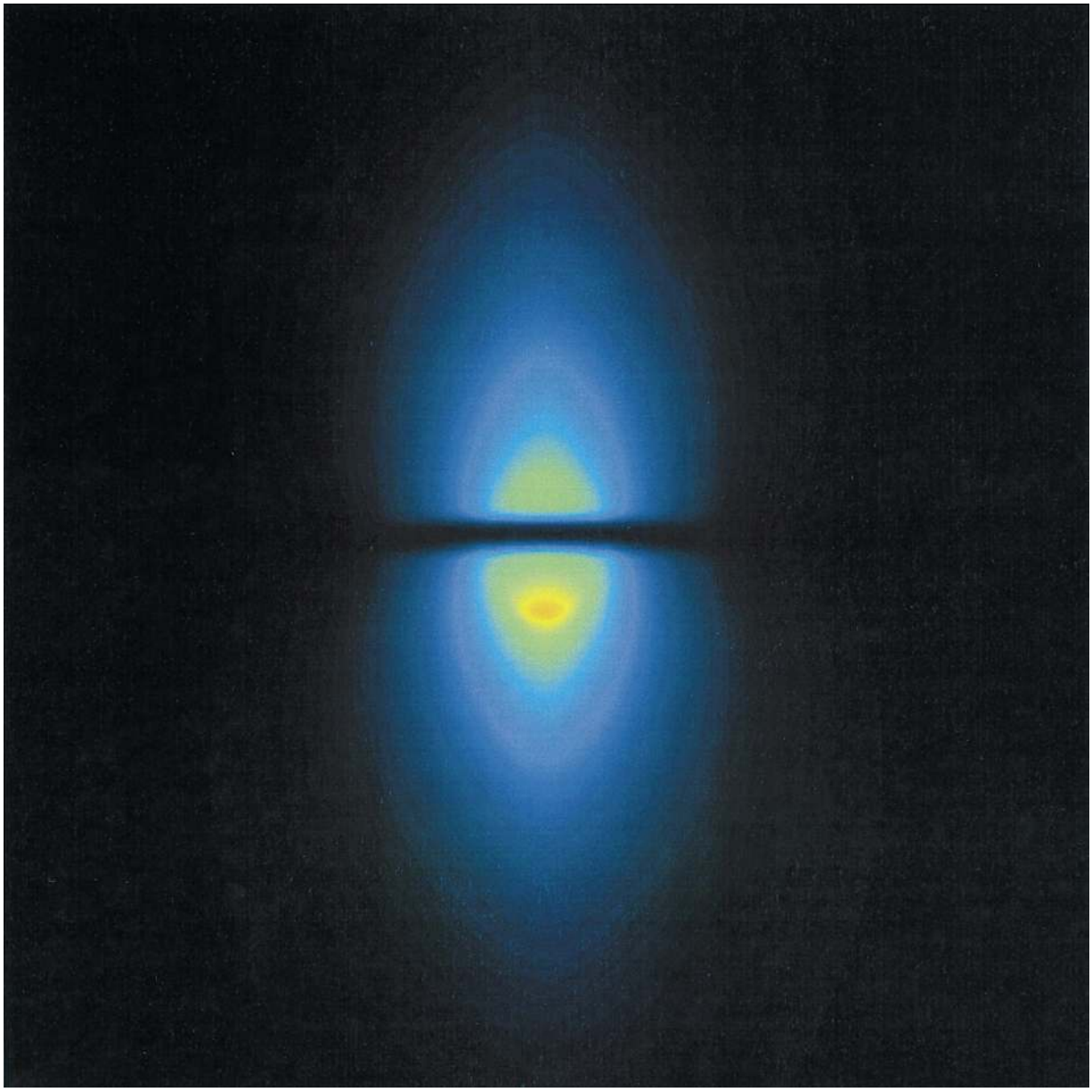

FIG. 4.—*V*-band model image of IRAS 17441−2411 based on the parameters in Table 1

mates the true luminosity of the central star in a bipolar nebula (see § 7).

The total mass of the circumstellar shell in the model is 2.9 (D/2.0 kpc) $M_\odot$, of which 0.13 (D/2.0 kpc) $M_\odot$ is in the disk and the rest is in the wind component. Note, however, that the model is not very sensitive to the outer radius, and thus if the density falls off more rapidly than inverse-square in the outer parts of the circumstellar shell, the total mass could be lower than is derived here. The extent of the density drop-off is constrained by the observed *IRAS* 60 μm flux, which requires dust of temperature as low as 40 K to be present. This implies that the dust envelope extends to at least 0.25 (D/2.0 kpc) pc, Beyond this distance, the density distribution is only constrained by the *IRAS* 100 μm upper limit. The minimum shell mass is therefore 1.5 (D/2.0 kpc) $M_\odot$ for the assumed dust-to-gas ratio. This implies that the progenitor has a minimum main-sequence mass of 2 $M_\odot$. Note that Corradi & Schwarz (1994) and Kastner et al. (1996), in their studies of bipolar PNs, find a correlation of bipolar structure with higher mass ($M > 1.5\ M_\odot$) progenitor stars; our results for IRAS 17441−2411 are consistent with this.

6. COMPARISON OF MODEL WITH OBSERVATIONS

The model works well in reproducing the SED of IRAS 17441−2411. In the current model the disk represents 4.4% of the total mass in the circumstellar shell. The distance to the source, for a given assumed luminosity, is uncertain by order of 5% to 10%, depending upon exactly how the model parameters are chosen to fit the main infrared part of the SED.

The match of the model to the V-band image is not perfect, but it is unlikely that this can be improved too much in a simple, general model. While the model predicts the correct ratio of peak brightnesses between the two lobes, it is not capable of reproducing the details seen in the optical image. In particular, the sharp edges to the main lobes are difficult to reproduced in a model using a simple

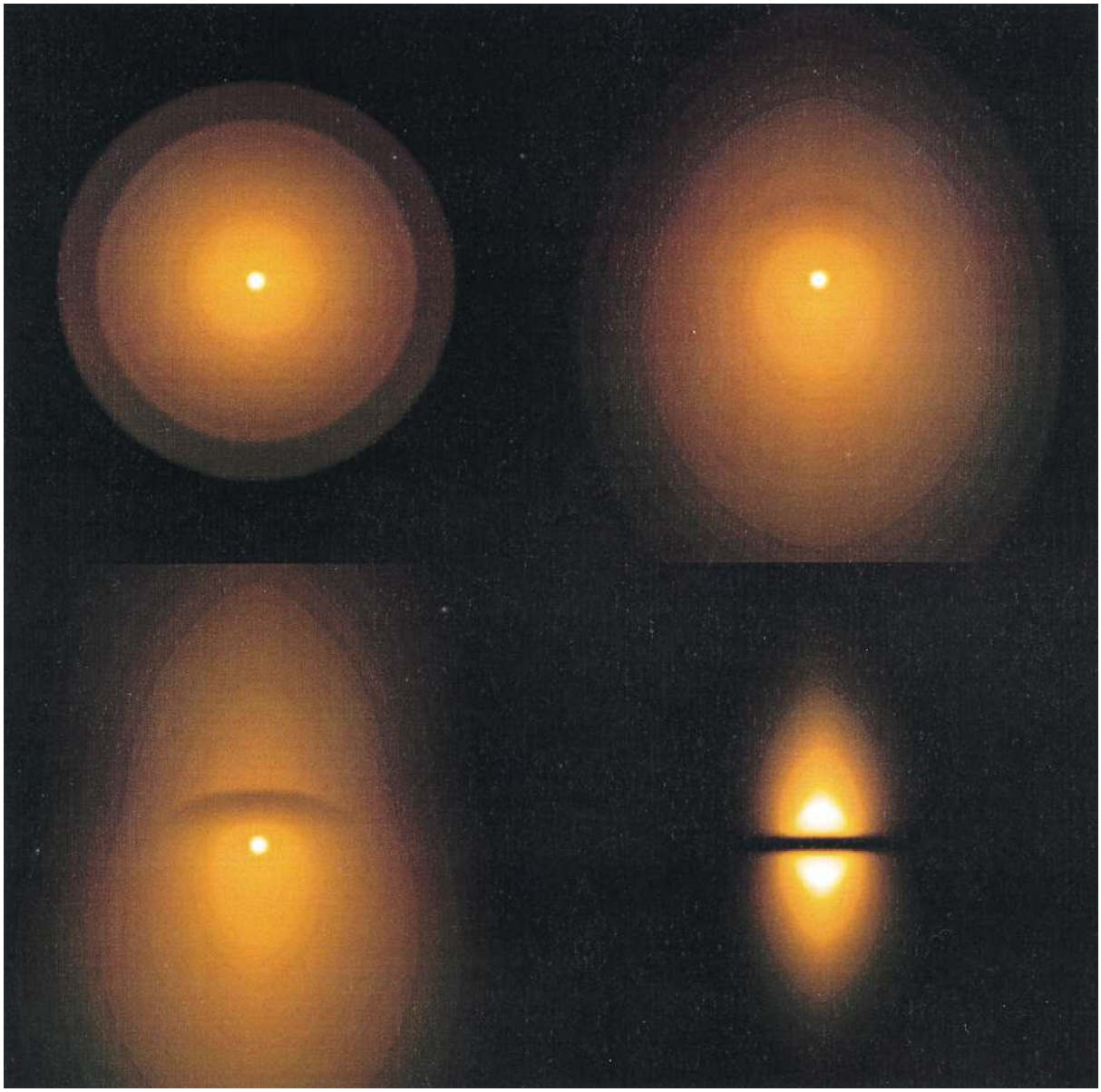

FIG. 5.—Model images of IRAS 17441−2411 viewed from four different angles: 0° (*upper left*), 30° (*upper right*), 60° (*lower left*), and 90° (*lower right*). For angles other than 90°, a logarithmic intensity scale is used.

continuous density function. The images produced by the model program predict reflection lobes that are slightly more open and fan-shaped than the actual appearance of the nebula. In order to produce an exact match to the observed morphology, a specific ad hoc density distribution would have to be used.

It is also clear that the smaller scale brightness variations within each lobe of the optical nebula and within the dark dust lane cannot be accommodated within the model. With further high-resolution observations at different wavelengths, it may be possible to deduce to what extent these features are due to variations in circumstellar extinction and to what extent they are due to local "clumps" of emitting material in the lobes.

One of the conclusions of our modeling effort is that a "disk" is needed to simulate the thin dark lane between the lobes of the *V*-band image. Since multiple scattering will enhance the intensity close to the central star and thus tends to connect the two lobes (Yusef-Zadeh, Morris, & White 1984), the need for this "disk" would be even greater if multiple scattering were included in the model.

In our model, we have simply assumed that the "disk" has the same inner radius as the wind. In reality, the disk could be much closer to the star. More specific properties of the disk will be clear from images at long wavelengths. Such images would preferentially "see" the warmer and denser regions of the dust shell.

7. DISCUSSION

While there have been previous efforts to model bipolar nebulae (e.g., the Monte Carlo calculations of Yusef-Zadeh et al. 1984), there has been no previous self-consistent radiation transfer model that attempts to fit both the scattered and emitted light components of bipolar nebulae. With the increasing availability of mid-IR imagers, the geometric and physical properties of bipolar nebulae can be much better

constrained by multiwavelength imaging. Our model represents a first step toward this direction.

Even before the availability of high-resolution mid-IR imaging data, a two-dimensional radiation transfer model will provide useful information on axial-symmetric systems using optical images and infrared photometry. For example, it is common practice to derive the luminosity of the central source of AGNs, young stellar objects, and PNs by integrating the flux under the SED. The underlying assumption is that the optical radiation reduced by extinction will be re-emitted in the infrared. In an axial-symmetric system, this assumption will yield erroneous results. This problem was first realized by Cohen & Kuhi (1977), but no quantitative calculations have been done.

We can use our model to illustrate quantitatively how the total flux observed from the central star changes with orientation. This can perhaps most easily be illustrated by examining the extreme orientations. The dust emission, which is generally optically thin except for wavelengths of ≤ 12 μm, is approximately the same for all angles of view. The observed stellar emission will obviously vary with viewing angle. At $i = 0°$ (pole-on), one will see both direct and scattered visible light from the star and full emission from the dust. If one multiplies the observed flux from the photospheric component by 4π, one would overestimate the luminosity of the system, because the stellar flux in the equatorial directions is already accounted for by the dust component. For angles from $i = 85°$ to $i = 95°$, the disk obscures the direct starlight and one would underestimate the total luminosity from the observed SED since only a fraction of the optical photons escaping from the polar directions are actually scattered toward us. At other i values we would observe both the reddened stellar emission and the full emission from the dust shell. The model calculations predict that the total observed flux from 17441−2411 would vary by +59% to −37%, with respect to $L_*/4\pi D^2$, from the polar to the equatorial directions. A more detailed discussion of this problem will be given separately (Volk et al. 1999).

At viewing angles where the disk does not obscure the star, the scattering lobes would be comparatively faint and very difficult to observe, given the limited dynamic range of detectors. Figure 5 shows simulated V-band images of the Silkworm Nebula viewed from different angles. In most directions, the nebulosity will be overwhelmed by the starlight, and it would be very difficult to tell that this is a bipolar nebula.

If such a bipolar morphology is typical of PPNs, we should expect most of them to appear stellar in optical images, and only of order 10% of them to show the bipolar morphology. The fact that we observe AFGL 2688 (the Egg Nebula), IRAS 17150−3224 (the Cotton Candy Nebula), and the Silkworm Nebula as bipolar nebulae is because of their favorable orientations. Most of the PPNs, if possessing similar intrinsic structures, will have ordinary (i.e., stellar) appearances in the visible and will only be identified as PPNs by their infrared properties. The exact fraction will depend upon the specific properties of the disk.

8. CONCLUSIONS

We have obtained high-resolution images of the bipolar PPN IRAS 17441−2411 with the *HST*. Two circular arcs can be seen around the outer parts of the nebula, suggesting that the star has undergone periods of enhanced mass loss during the preceding AGB phase. This is the third example of a bipolar PPN to show such arcs (the others being AFGL 2688 and IRAS 17150−3224), which suggests that enhanced episodes of mass loss are not uncommon. Harpaz, Rappaport, & Soker (1997) have recently suggested an eccentric binary orbit model as a mechanism to vary periodically the isotropic mass outflow and produce the arcs. However, with the present total of three PPN with concentric arcs, the observed frequency is much higher than the very low frequency (0.3%) predicted by the authors.

The two lobes of the nebula are separated by a thin dust lane, which is attributed to a thin circumstellar "disk." By fitting the observed SED and V-band image of the nebula with a two-dimensional radiation transfer model, we are able to derive the physical properties of the AGB wind and the "disk." The spectacular appearance of this object is the fortuitous result of it being viewed almost edge-on. We suggest that there exist other PPNs of similar intrinsic structure whose optical images show little or no sign of their bipolarity.

We thank M. Bobrowsky for communicating his results on IRAS 17441−2411. This work is supported by a grant to S. K. by the Natural Sciences and Engineering Research Council of Canada, and by a grant to B. J. H. by NASA through grant number GO-06565.01-95A from the Space Telescope Science Institute, which is operated by the Association of Universities for Research in Astronomy, Inc., under NASA contract NAS 5-26555.

REFERENCES

Bobrowsky, M., Meixner, M., & Skinner, C. J. 1998, in ASP Conf. Ser., 1997 Pacific Rim Conference On Stellar Astrophysics, ed. K. L. Chan, K. S. Cheng, & H. P. Singh (San Francisco: ASP), 19
Casertano, S. 1997, in 1997 *HST* Calibration Workshop, ed. S. Casertano et al. (Baltimore: STScI), 327
Cohen, M., & Kuhi, L. V. 1977, ApJ, 213, 79
Corradi, R., & Schwarz, H. 1994, A&A, 293, 871
Fruchter, A. S., & Hook, R. N. 1997, Proc. SPIE, 3164, 120
Harpaz, A., Rappaport, S., & Soker, N. 1997, ApJ, 487, 809
Hrivnak, B. J. 1997, in IAU Symp. 180, Planetary Nebulae, ed. H. J. Habing & H. Lamers (Dordrecht: Kluwer), 303
Hrivnak, B. J., & Kwok, S. 1991, ApJ, 368, 564
Hu, J. Y. Slijkhuis, S., de Jong, T., & Jiang, B. W. 1993, A&AS, 100, 413
Hu, J. Y., te Lintel Hekkert, P., Slijkhuis, S., Baas, F., Sahai, R., & Wood, P.R. 1994, A&AS, 103, 301
Kastner, J. H., Weintraub, D. A., Gatley, I., Merrill, K. M., & Probst, R. G. 1996, ApJ, 462, 777
Kwok, S. 1993, ARA&A, 31, 63
Kwok, S., Hrivnak, B. J., Zhang, C. Y., & Langill, P. L. 1996, ApJ, 472, 287
Kwok, S., Su, K. Y.-L., & Hrivnak, B. J. 1998, ApJ, 501, 117
Kwok, S., Volk, K., & Bidelman, W. P. 1997, ApJS, 112, 557
Neckel, Th., & Klare, G. 1980, A&AS, 42, 251
Ohashi, N., Kawabe, R. Hayashi, M., & Ishiguro, M. 1991, AJ, 102, 2054
Sahai, R., et al. 1998, ApJ, 493, 301
Spagna, G. F., Leung, C. M., & Egan, M. P. 1991, ApJ, 379, 232
Volk, K., Su, K. L., & Kwok, S. 1999, in preparation
Weintraub, D. A., Huard, T., Kastner, J. H., & Gatley, I. 1998, ApJ, 509, in press
Yusef-Zadeh, F., Morris, M., & White, R. L. 1984, ApJ, 278, 186